iScience

Article

Single-cell transcriptomic reveals the peritoneal microenvironmental change in long-term peritoneal dialysis patients with ultrafiltration failure

Graphical abstract

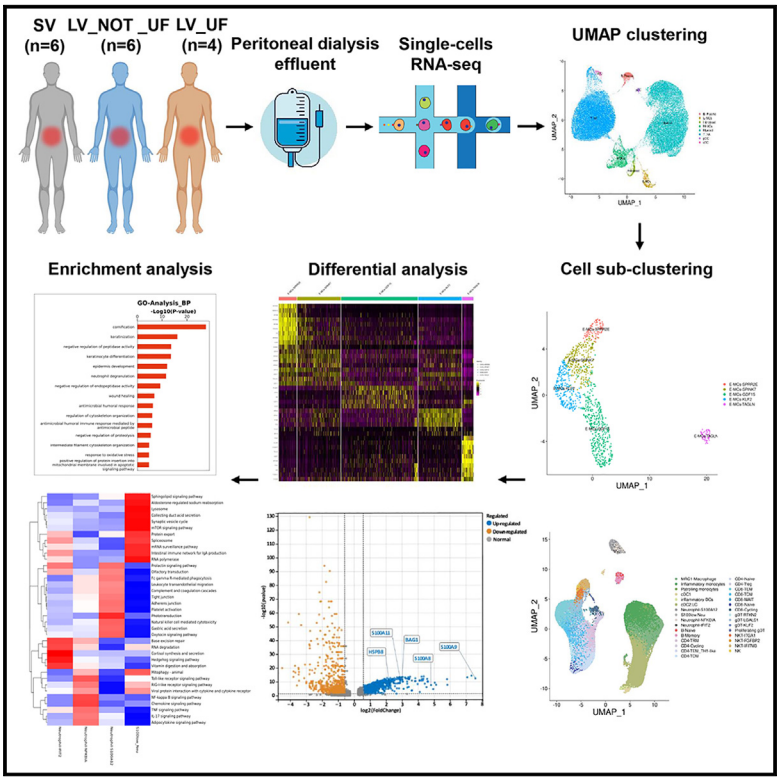

Highlights

- scRNA-seq showed peritoneal microenvironment in patients with peritoneal dialysis
- scRNA-seq identified neutrophil increase in patients with ultrafiltration failure
- A higher abundance of E-MCs was found in patients with ultrafiltration failure
- Patients with ultrafiltration failure revealed reduced M-MCs and *AQP1* expression

Authors

Xiangwen Diao, Cuixia Zhan, Hongjian Ye, ..., Haiping Mao, Wei Chen, Xiao Yang

Correspondence

yxiao@mail.sysu.edu.cn

In brief

Body substance sample; Integrative aspects of cell biology; Microenvironment; Transcriptomics

Diao et al., 2024, iScience *27*, 111383
December 20, 2024
https://doi.org/10.1016/j.isci.2024.111383

CellPress

iScience

CellPress
OPEN ACCESS

Article

Single-cell transcriptomic reveals the peritoneal microenvironmental change in long-term peritoneal dialysis patients with ultrafiltration failure

Xiangwen Diao,[1,4] Cuixia Zhan,[2,3,4] Hongjian Ye,[2,3] Haishan Wu,[2,3] Chunyan Yi,[2,3] Jianxiong Lin,[2,3] Haiping Mao,[2,3] Wei Chen,[2,3] and Xiao Yang[2,3,5,*]

[1]Department of Emergency, The First Affiliated Hospital, Sun Yat-Sen University, Guangzhou 510080, Guangdong, China
[2]Department of Nephrology, The First Affiliated Hospital, Sun Yat-sen University, Guangzhou 510080, Guangdong, China
[3]NHC Key Laboratory of Clinical Nephrology (Sun Yat-Sen University) and Guangdong Provincial Key Laboratory of Nephrology, Guangzhou 510080, Guangdong, China
[4]These authors contributed equally
[5]Lead contact
*Correspondence: yxiao@mail.sysu.edu.cn
https://doi.org/10.1016/j.isci.2024.111383

SUMMARY

The microenvironmental changes in peritoneal dialysis effluent (PDE) after long-term vintage (LV) of PD in patients with ultrafiltration failure (LV_UF) are unclear. Single-cell sequencing revealed that peritoneal neutrophils were elevated in LV_UF patients, while MRC1-macrophage subcluster decreased compared with PD patients with short vintage (SV) and LV without ultrafiltration failure (LV_NOT_UF). Compared with the LV_NOT_UF group, the upregulated differentially expressed genes (DEGs) of monocytes/macrophages in the LV_UF group were involved in inflammatory response and EMT progress. LV_UF patients had a higher proportion of epithelial-like mesothelial cells (E-MCs), which were characterized by autophagy activation, inflammation, and upregulation of neutrophil- and autophagy-related DEGs compared to the LV_NOT_UF group. Additionally, mesenchymal-like MCs and *AQP1* expression were reduced in the LV_UF group compared with the other groups. Both neutrophils and monocytes/macrophages interacted with MCs. Our study provides insights into the roles of peritoneal mesothelial cells and inflammatory cells in PD patients with UF.

INTRODUCTION

Peritoneal dialysis (PD), one of the renal replacement treatments, uses the peritoneal membrane as a dialyzing membrane to exchange water and solutes in a hyperosmotic environment.[1] The three-pore model (TPM) of peritoneal transport derived from capillary physiology has been recognized as a valuable method for describing transperitoneal exchange of solutes and water.[2,3] According to the classical TPM, the peritoneal membrane includes ultrasmall, small, and large pores.[4] On the other hand, the distributed model of peritoneal transport extends the peritoneal barrier to include peritoneal parenchymal cells, mesenchymal cells, and stromal molecules, all of which influence peritoneal fluid and solute transport.[5,6] Years of PD treatment results in the functional and constructional changes of the peritoneal membrane, which affects the clinical outcome of patients.[7] Decreased fluid clearance is the most common problem of the peritoneal membrane and is considered an important screening tool for membrane dysfunction.[7] Recent guidelines classify membrane dysfunction into three categories,[7] but the specific mechanisms leading to the pathophysiological changes in the peritoneum remain unclear.

The peritoneal effluent is readily available compared to the peritoneal tissue, which is invasive to patients. Peritoneal dialysis effluent (PDE) is the fluid that flows out after completing substance exchange within the patient's body during PD using dialysate. Specifically, the PDE contains various peritoneal cells, which provide an alternative to defining the complete cellular and molecular composition of peritoneal cells. Single-cell RNA sequencing (scRNA-seq) is a powerful approach for transcriptome-wide analysis of differential gene expression and definition of cellular composition in a single cell.[8,9] Cells obtained from PDE were evaluated using single-cell transcriptome and found that hyperglycolysis was responsible for the alteration of mesothelial cells (MCs) and peritoneal fibrogenesis,[10] and macrophages had the property of promoting fibrosis.[11] In addition, the population of fibroblasts obtained from the patients receiving PD showed a proinflammatory role and a crosstalk with immune cells.[12] However, these studies focused on patients with long- and short-term PD, lacking further heterogeneous analysis between patients with ultrafiltration failure (UF) or not. We hypothesize that the alterations of molecules, peritoneal tissue, and cells contribute to the transformation of peritoneal function in patients undergoing

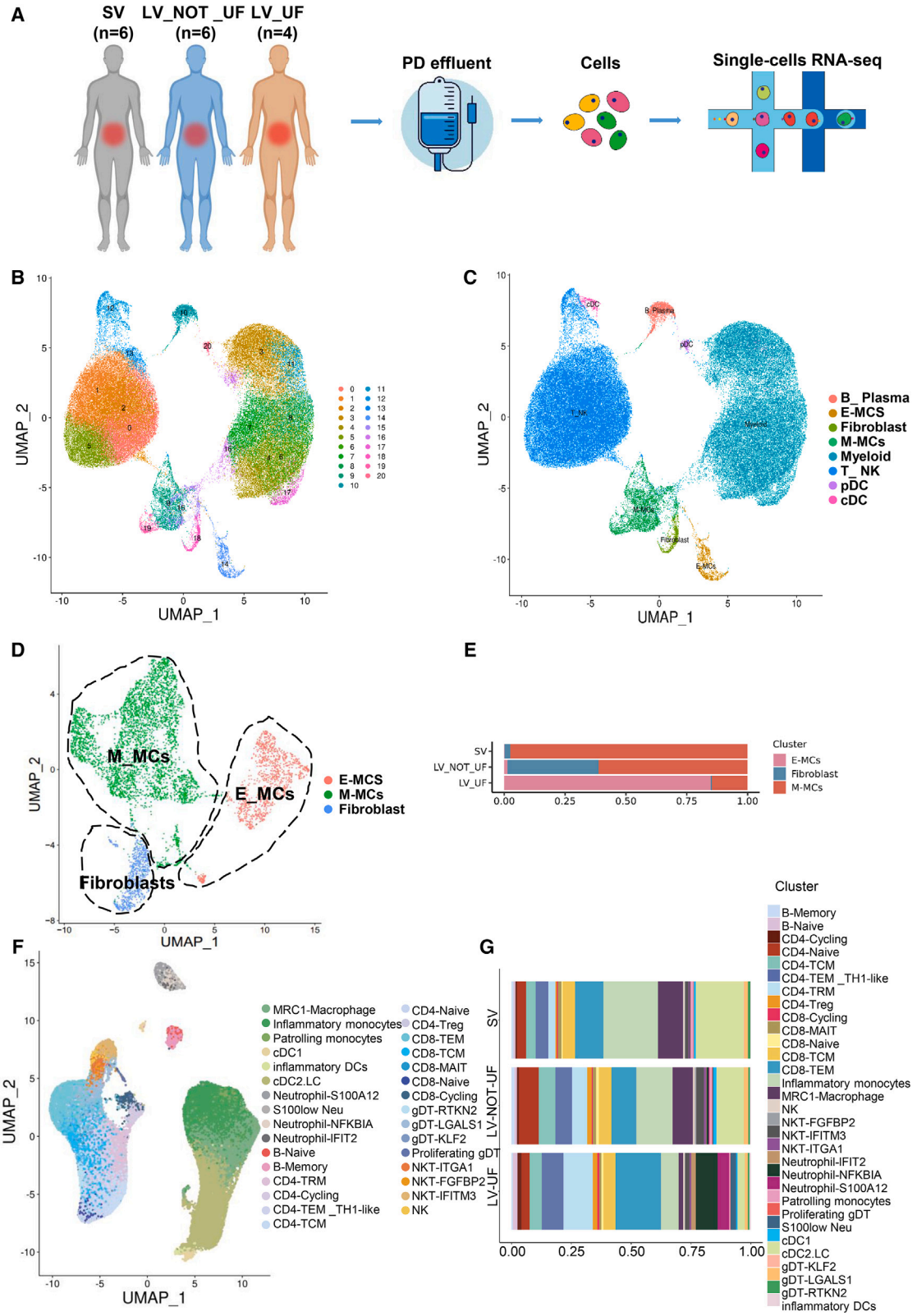

(legend on next page)

long-term PD. Here, scRNA-seq was performed to analyze the cell composition and transcriptome characteristics of peritoneal effluent obtained from PD patients across short vintage (SV), long vintage without ultrafiltration failure (LV_NOT_UF), and long vintage with ultrafiltration failure (LV_UF) to demonstrate the changes of peritoneal microenvironment.

RESULTS

Single-cell transcriptomic analysis reveals changes in cell composition of PDE

The median PD vintage of the SV, LV_NOT_UF, and LV_UF groups were 5 months (range:1.0–6.0 months), 137 months (range: 92–189 months), and 132 months (range: 120–161 months) respectively, with no significant differences in age (38.3 ± 21.5 years, 45.7 ± 10.6 years, and 41.0 ± 16.7 years, $p > 0.05$) and gender (male%: 33.3%, 50.0%, and 25.0%, $p > 0.05$). To better understand the heterogeneity among patients received PD, we applied scRNA-seq to characterize the cell composition and transcriptomic status of peritoneal fluid from individuals in SV, LV_NOT_UF, and LV_ UF phases (Figure 1A). We applied the Seurat package for cell normalization and cell filtering considering the mitochondria percentage, minimum, and maximum gene numbers (Figures S1A and S1B). After filtering, 103,638 cells were analyzed, including 47,943 in the SV group, 39,309 in the LV_NOT UF group, and 16,386 in the LV_UF group (Table S2). The central cells were further analyzed, and the top 2,000 genes with the highest variable were subjected to subsequent analysis (Figure S1C). Notably, the cells were divided into 21 clusters (Figure 1B) and then annotated into 8 major cell types based on highly expressed genes using unsupervised UMAP clustering (Figures 1C and S1D), including epithelial-like mesothelial cells (E-MCs), mesenchymal-like mesothelial cells (M-MCs), fibroblasts, plasma B cells, conventional dendritic cells (cDC), plasmacytoid dendritic cells (pDC), natural killer T (T_NK) cells, and myeloid cells. To better demonstrate the cell function of these cell types, cells were classified as non-immune and immune profiles. The non-immune profiles included E-MCs, M-MCs, and fibroblast (Figure 1D), and the other cells were classified as immune profiles. Expectedly, cell types' composition was accumulated differently in the three PD states. For example, E-MCs strongly accumulated in the LV_UF group, fibroblast remarkably enriched in the LV_NOT_UF group, and M-MCs concentrated in the SV group (Figure 1E). The proportion of M-MCs gradually reduced from SV to LV_UF (Figure 1E). On the contrary, E-MC cells showed an increase. The immune profiles were further categorized into 31 heterogeneous subtypes: MRC1-Macrophage, 2 subtypes for monocyte, 3 subtypes for DCs, 4 subtypes for neutrophil, 2 subtypes for B cells, 6 subtypes for CD4 T cells, 5 subtypes for CD8 T cells, 4 subtypes for gDT cells, and 4 subtypes for NK cells. (Figure 1F). Heterogeneity in the abundance of different immune cell subpopulations in the three PD states was prominent (Figure 1G). In short, the cell composition of PDE was altered after UF, suggesting that cellular heterogeneity may be associated with pathological changes in different states of PD.

Heterogeneity analysis of E-MC subclusters in PDE

Previous studies have evaluated single-cell transcriptomes of MCs in normal peritoneal biopsy and effluent from patients accepting PD, which reported that long-term PD increased the expression of epithelial-mesenchymal transition (EMT)-associated marker genes.[10,12] However, the characteristics of MC cell-type heterogeneity in PD drainage fluid are absent. In our study, MCs were annotated into E-MCs and M-MCs to further investigate the heterogeneous changes of MCs in different PD status. Among these, a previous study reported that E-MCs possess epithelial cell features such as becoming polarized upon cell-cell contact and resting upon a basement membrane.[13] Notably, E-MCs primarily appeared in the LV_UF group, with a tiny cell population in the SV and LV_NOT_UF groups (Figure 2A). We then extracted relevant data of E-MCs, which yielded five subclusters by UMAP that we termed E-MCs-SPRR2E, E-MCs-SPINK7, E-MCs-GDF15, E-MCs-KLF2, and E-MCs-TAGLN (Figure 2B and Table S3). The E-MCs-SPRR2E and E-MCs-SPINK7 strongly expressed keratin genes, including *KRT6A*, *KRT6B*, *KRT16,* and *KRT17* (Figure 2C), which are abundantly expressed in epithelial cells that support cell polarization and cellular adherent junctions.[14] Furthermore, GO analysis showed that E-MCs-SPRR2E and E-MCs-SPINK7 participated in cornification, keratinocyte differentiation, and epidermis development (Figures 2D and 2E). The top 20 pathway enrichment analyses also suggested that E-MCs-SPRR2E and E-MCs-SPINK7 were enriched in autophagy and mitophagy pathways (Figures S2A and S2B). Interestingly, several subclusters, including E-MCs-SPRR2E, E-MCs-SPINK7, E-MCs-GDF15, and E-MCs-TAGLN, were remarkably enriched in the neutrophil degranulation pathway (Figures 2D and 2E; Figures S2C and S2D). On the other hand, QUSAGE analysis revealed that E-MCs-TAGLN was mainly enriched in p53 pathway, PI3K/AKT/mTOR signaling pathway, wnt beta-catenin signaling, and EMT pathways (Figure 2F). Taken together, these results suggested heterogeneity

Figure 1. Identification of 8 cell types with diverse annotations based on single-cell RNA sequencing (scRNA seq) data

(A) Schematic of scRNA-seq sample preparation.

(B) The distribution of all 21 identified cell clusters is visualized by Uniform manifold approximation and projection (UMAP).

(C) Cells from PDE are annotated into 8 cell types according to the expressions of marker genes.

(D) Non-immune cell types are visualized by UMAP, including epithelial-like mesothelial cells (E-MCs), mesenchymal-like MCs (M-MCs), and fibroblast.

(E) Percentage of 3 non-immune cell types (E-MCs, M-MCs, and fibroblast) in the SV, LV_NOT_UF, and LV_UF groups. The horizontal axis is cell proportion, and the vertical axis is group.

(F) UMAP distribution map of immune cell types identified in PDE.

(G) The percentage of immune cell types identified in PDE in the SV, LV_NOT_UF, and LV_UF groups is shown. The horizontal axis is cell proportion, and the vertical axis is group.

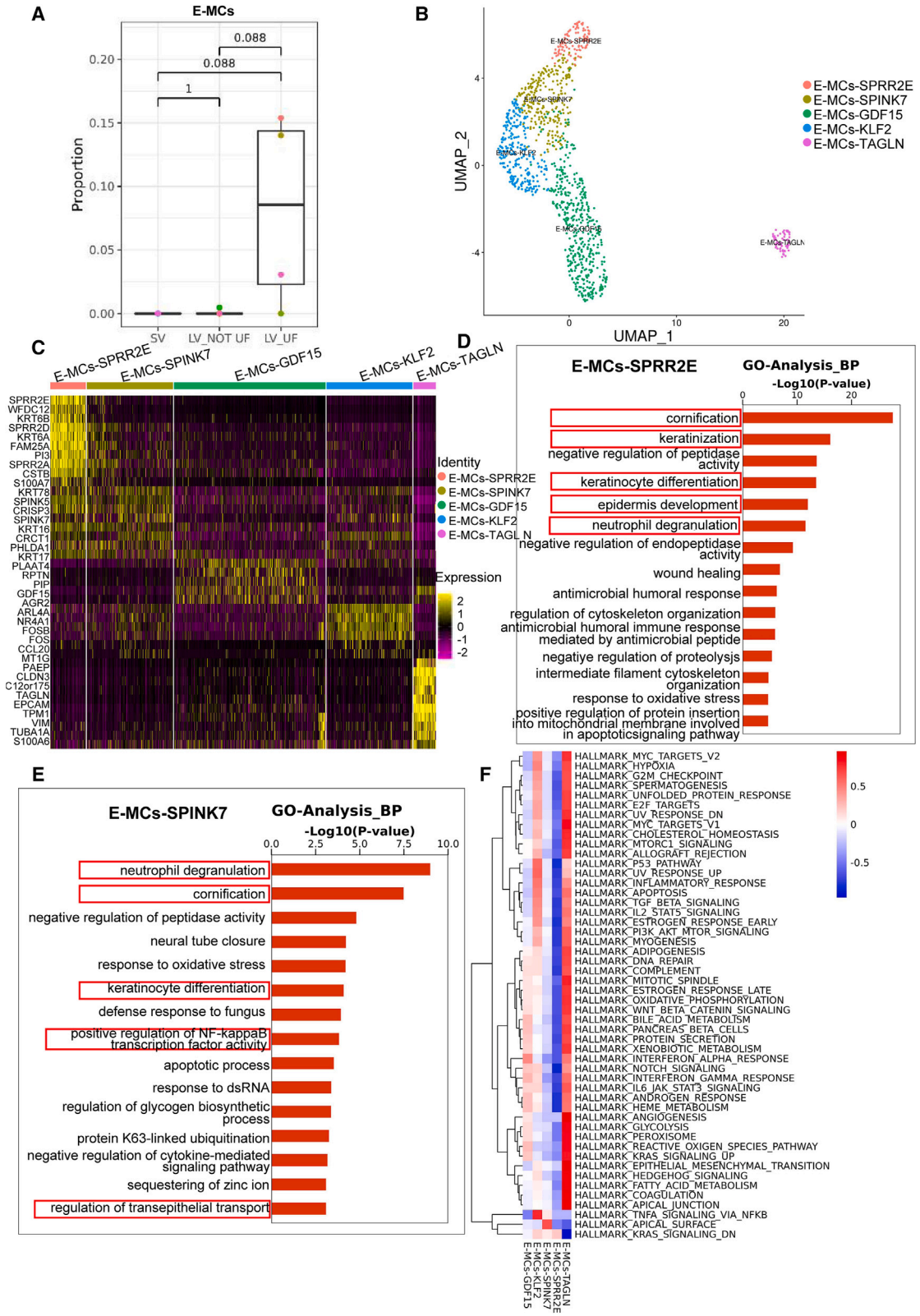

(legend on next page)

among subclusters of E-MCs, and the elevation of E-MCs in PDE of LV_UF patients may reflect the increasing denudation of MCs possessing epithelial phenotypes from peritoneal membrane.

E-MCs exhibit enrichment in autophagy-related pathways

Given our findings that E-MCs-SPRR2E and E-MCs-SPINK7 are associated with autophagy (Figures S2A and S2B), we therefore further explore the association between autophagy and E-MCs subtypes. The expression of autophagy-associated genes in E-MCs was visualized by bubble plot (Figure 3A). *MAP1LC3B*, *RAB7A*, and *BECN1*, which primarily participated in the formation of autophagosome,[15,16] showed an enrichment in E-MCs. As evidenced in the heatmap, E-MCs were strongly enriched in autophagy (other and animal), mitophagy, and apoptosis pathways (Figure 3B). Similarly, GO and KEGG analyses also exhibited the involvement of E-MCs in various autophagy-related pathways, including mitophagy, macroautophagy, and autophagosome assembly (Figures 3C and 3D). To sum up, these results demonstrated an enrichment of autophagy-related pathways within E-MCs.

E-MCs show inflammatory characteristics

E-MCs exhibited pro-inflammatory features. As shown in Figure S3A, the pro-inflammatory-associated marker genes were greatly stimulated in E-MCs, such as *LCN2* (an innate immune protein that regulates immune responses),[17] *S100A8/9* (bound to *TLR4* and inducing pro-inflammatory cytokines and chemokines),[18,19] *TICAM1* (participates in *TLR3* mediated proinflammatory cytokine),[20] and *CXCL16* (encourages monocyte and T cell attachment to endothelial cells).[21] Interestingly, E-MCs also displayed an increase in anti-inflammatory gene expression, including *IL1RN* (an antagonist of proinflammatory cytokines)[22] and *LGALS9* (the family of lectins that have anti-inflammatory activity)[23] (Figure S3A). Different subtypes of E-MCs exhibit different inflammatory properties, with the E-MCs-KLF2 subtype being predominantly pro-inflammatory and highly expressed *IFNG*, *GZMA*, *IL1A*, and *CCL20*, while the E-MCs-TAGLN subtype has a two-sided effect of inflammation (Figure S3B). In short, our results elucidate the pro-inflammatory and anti-inflammatory characteristics in E-MCs.

Neutrophil degranulation and autophagy within E-MCs may be activated in the LV_UF group

To further characterize the transcriptional differences of E-MCs in PDE from patients of the LV_NOT_UF and LV_UF groups, we performed a DEG analysis. Based on 5210 genes within E-MCs, 3481 DEGs were identified, including 769 upregulated and 2712 downregulated DEGs in the LV_UF group compared to the LV_NOT_UF group (Figure 4A). Interestingly, the upregulated DEGs in the LV_UF group compared to the LV_NOT_UF group were found to be involved in pathways of neutrophil degranulation and autophagy (Figure 4B). The downregulated DEGs in the LV_UF group were associated with collagen fibril and ECM organization (Figure 4C). Collectively, these findings indicate that neutrophil degranulation and autophagy within E-MCs may be activated in the LV_UF group.

AQP1 downregulation in PDE may be a biomarker for UF

The water channel Aquaporin 1 (*AQP1*) is validated to be responsible for approximately 50% of ultrafiltration in 2-h hypertonic dwell[24] and plays an important role in UF in PD according to the TPM.[25] Therefore, we wondered whether scRNA-seq data of PDE could laterally verify the function of *AQP1*. As illustrated in Figure S3C, *AQP1* was predominantly expressed in non-immune cells (E-MCs, M-MCs, and fibroblast), with little expression in immune cells. Moreover, *AQP1* expression was significantly reduced in E-MC compared to M-MCs and fibroblast (Figure 4D). Notably, *AQP1* was found a lower expression in the LV_UF group compared to the LV_NOT_UF and SV groups (Figure 4E), suggesting that the downregulation of *AQP1* in PDE may be a specific molecular event in UF.

M-MCs respond to UF through participating in EMT, fibrosis, and inflammation

In contrast to the increase in E-MCs abundance, our scRNA-seq data revealed that PDE-derived M-MCs showed a reduction in the LV_UF group compared with SV group (Figure 5A). We performed sub-cluster analysis for M-MCs alone that were annotated into the 9 clusters, including M-MCs-IL6, M-MCs-SLC7A4, M-MCs-SERPINB2, M-MCs-RGCC, M-MCs-MAFB, M-MCs-proliferation, M-MCs-HLA-DRB1, M-MCs-MMP7, and M-MCs-POSTN based on the known marker genes (Figure 5B and Table S4). Pseudotime trajectory was performed for M-MCs, and the results showed that M-MCs deveplopment followed 3 differentiation directions (Figure 5C). MCs with mesenchymal features are characterized by higher motility and the capacity to produce ECM, thus contributing to fibrosis.[26] The M-MCs-POSTN and M-MCs-RGCC were primarily accumulated in states 1 and 4 and showed an enrichment in ECM organization, cell adhesion, cell migration, oxidative phosphorylation, collagen fibril organization, actin cytoskeleton organization, and neutrophil degranulation, suggesting that EMT and fibrosis occurred in the peritoneal membrane (Figures S4A and S4B). The distributions of M-MCs from all three PD periods (SV, LV_NOT_UF, and LV_UF) in the pseudotime trajectory are also shown in Figure 5C. Meanwhile, *COL1A1*, *COL3A1*, and vimentin (*VIM*), well-known mesenchymal signatures, were abundantly enriched in M-MCs and fibroblasts (Figure 5D), further confirmed

Figure 2. Heterogeneity analysis of E-MC subclusters in PDE

(A) Proportion of E-MCs in the SV, LV_NOT_UF, and LV_UF groups. The Wilcoxon Rank-Sum test was used to calculate the statistical difference. Data are represented as mean ± SD.

(B) E-MCs were re-clustered into five sub-cell types and displayed by the UMAP plot.

(C) Heatmap revealing the expression of marker genes in five subpopulations of E-MCs.

(D and E) GO enrichment analysis was performed based on the expressed marker genes in E-MCs-SPRR2E (D) and E-MCs-SPINK7 (E) cell types.

(F) Hallmark pathway enrichment of five E-MC subclusters analyzed by QuSAGE are shown by heatmap.

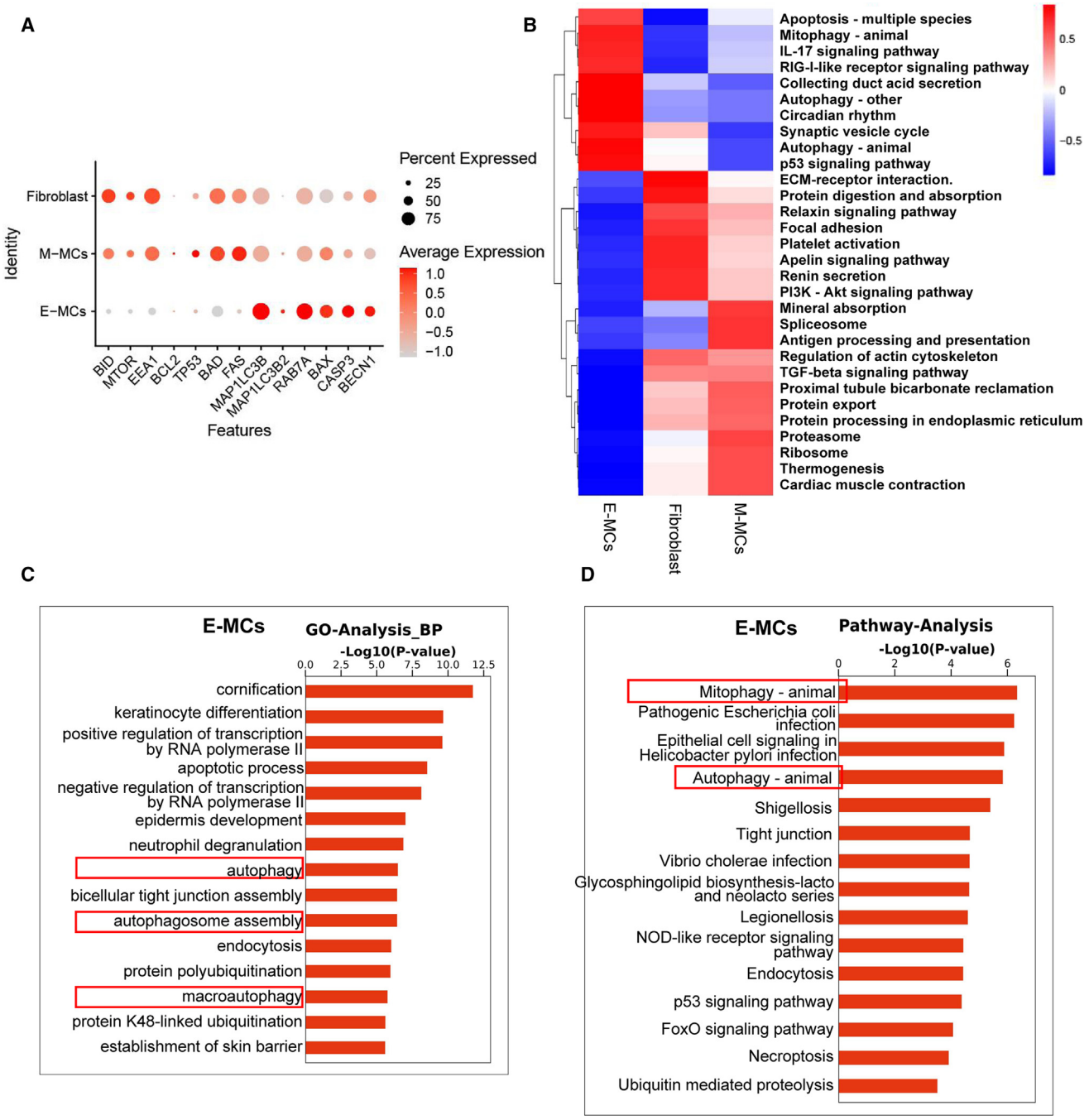

Figure 3. E-MCs exhibit autophagy activation

(A) Bubble map shows the expression of autophagy-associated marker genes in E-MCs, M-MCs, and fibroblasts. The bubble size represents the percentage of gene expression in the relevant cell types, and the color indicates average gene expression.

(B) QuSAGE analysis reveals the pathway enrichment of gene sets in E-MCs, M-MCs, and fibroblasts.

(C) GO enrichment analysis of E-MCs shows the association between E-MCs and autophagy.

(D) KEGG enrichment of E-MCs was performed based on the expressed marker genes in E-MCs.

that the mesenchymal-like signatures of MCs contributed to develop fibrosis. M-MCs-proliferation population showed an enrichment in cell division and cell cycle and participated in the modulation of the mitotic cell cycle (Figure S4C). Moreover, M-MCs-IL6 and M-MCs-MAFB were found to be associated with the TNF signaling pathway, Th17 cell differentiation, and MAPK signaling pathway, as evidenced in the KEGG analysis (Figures S4D and S4E), indicating the occurrence of

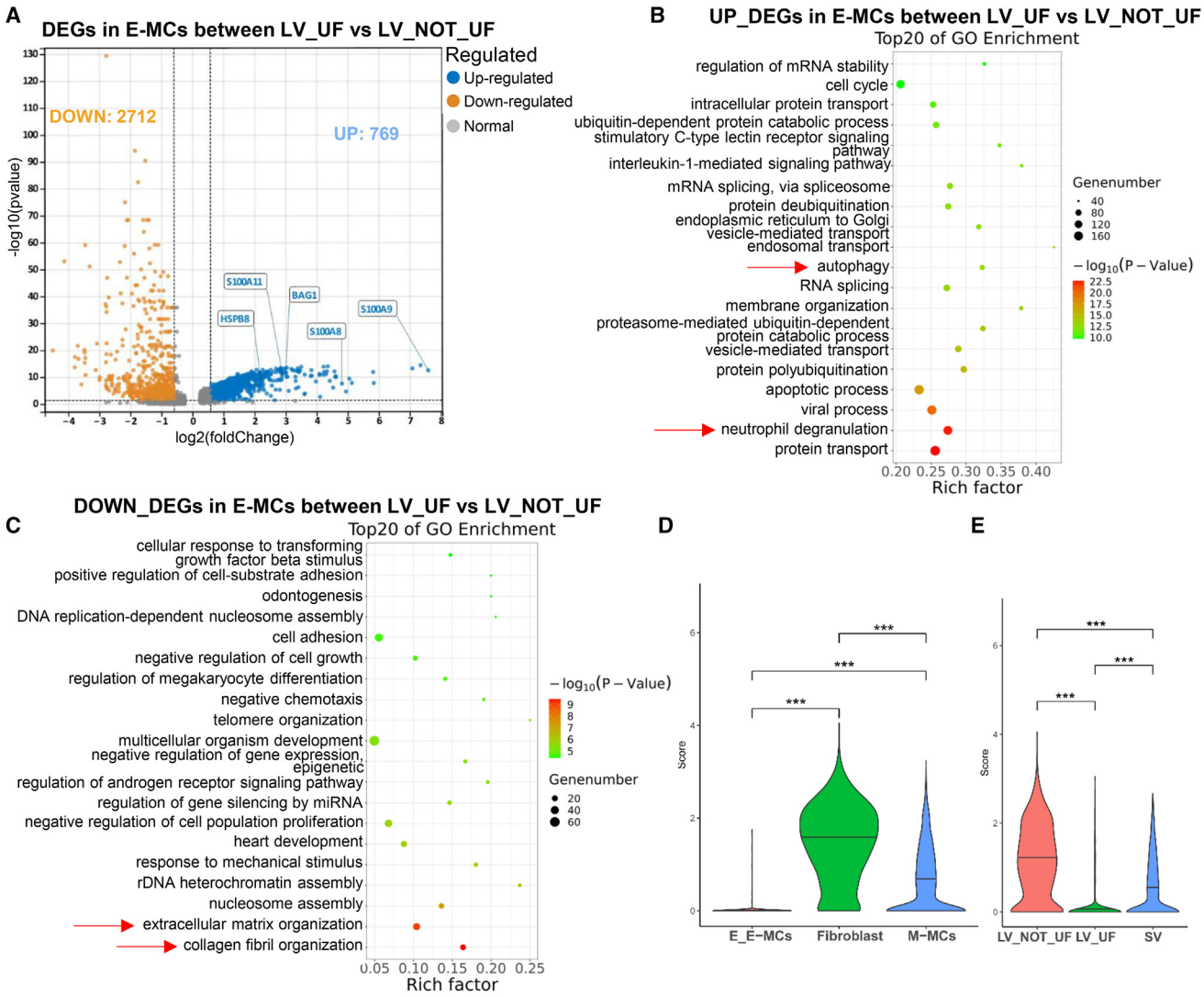

Figure 4. Pathways of neutrophil degranulation and autophagy within E-MCs may be activated in the LV_UF group

(A) Volcano map of DEGs in E-MCs between the LV_ UF and LV_NOT_UF groups.

(B and C) The bubble map shows the top 20 GO enrichment of upregulated DEGs (B) and downregulated DEGs (C) in E-MCs between the LV_ UF vs. LV_NOT_UF groups.

(D) Violin map shows that in the three non-immune cells (M-MCs, E-MCs, and fibroblast), *AQP1* expression was significantly decreased in E-MCs compared to M-MCs and fibroblast. The Wilcoxon Rank-Sum test was used to calculate the statistical difference. ***$p < 0.001$.

(E) Violin map shows that *AQP1* expression in the three non-immune cells (M-MCs, E-MCs, and fibroblast) of peritoneal mesenchyme was significantly reduced in the LV_UF group compared to the other groups. The Wilcoxon Rank-Sum test was used to calculate the statistical difference. ***$p < 0.001$.

inflammatory response in M-MCs. A heatmap of inflammatory gene expression in different M-MCs subtypes is shown in Figure S3D. Different specific subtypes of M-MCs exhibited heterogeneity, meaning that the expression patterns of inflammatory genes are different. Interestingly, we found that M-MCs-SLC7A4 showed the character of E-MCs, such as cornification and epidermis development (Figure S4F).

We next performed DEG analysis for M-MCs and sought to explore the differential response of M-MCs to PD across SV, LV_NOT_UF, and LV_UF. The GO analysis showed that the DEGs were mainly enriched in ECM organization, positive regulation of cell migration, neutrophil degranulation, and collagen fibril organization, indicating progressing EMT and fibrosis in LV_NOT_UF (Figure S4G). In addition, the GO term of DEGs revealed M-MCs in LV_UF involved in cornification, epidermis development, NF-κB signaling, and IFN signaling pathway (Figure S4H). These results demonstrated that MCs acquired mesenchymal phenotypes and contributed to EMT, fibrosis, and inflammation.

Immunomodulatory characteristics of neutrophils and their crosstalk with MCs

In previous reports, scRNA-seq data revealed the accumulation of leukocytes such as monocyte and NK cells[12] but lacking

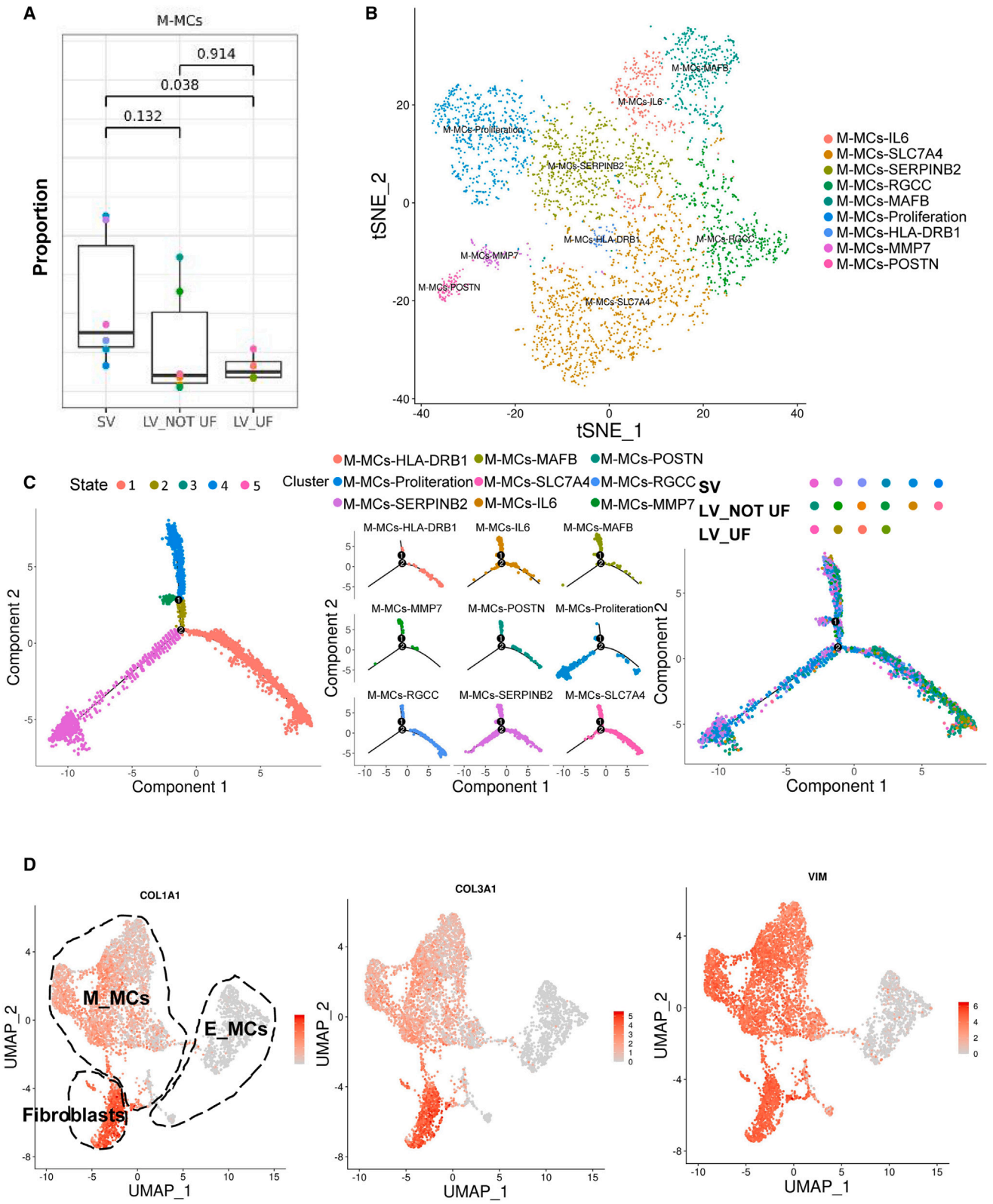

(legend on next page)

neutrophils. However, neutrophil was detected in peritoneal effluent cells and showed an exceptional enrichment in our study. Although the neutrophil abundance increased in LV_UF, no significant differences were found compared to the SV or LV_NOT_UF groups (Figure 6A). The neutrophil was subclustered into 4 subtypes by UMAP, including neutrophil-S100A12, S100^{low} neutrophil, neutrophil-NFKBIA, and neutrophil-IFIT2 (Figure 6B). Neutrophil-NFKBIA strongly enriched inflammation-associated pathways, such as the Toll-like receptor signaling pathway, NF-κB signaling pathway, IL-17 signaling pathway, and TNF signaling pathway (Figure 6C). Neutrophil-related DEGs of E-MCs were upregulated in the LV_UF group (Figure 4A), and the GO enrichment analysis supported the association between neutrophils and E-MCs. For example, neutrophil-IFIT2 enriched in "negative regulation of mesenchymal to epithelial transition involved in metanephros morphogenesis" and "metanephric mesenchymal cell proliferation involved in metanephros morphogenesis" (Figure 6D). Marker genes, including *S100A8*, *S100A9*, and *S100A11*, were highly expressed in neutrophil-S100A12 (Figure 6E) that correspond with the upregulated DEGs in E-MCs (Figure 4A). As ligand cells, neutrophil-S100A12 also interacted with E-MCs in the LV_UF group (Figure 7A). Furthermore, neutrophil-NFKBIA as ligand cells expressed *CXCL8* to pair with CXCR2 receptor, which was expressed in M-MCs such as M-MCs-SERPINB2, M-MCs-RGCC, M-MCs-SLC7A4, and M-MCs-IL6 in the LV_UF group (Figure 7B). *CXCR2* is a G-protein-coupled receptor for the human CXC chemokines *CXCL1*, *CXCL2*, *CXCL3*, *CXCL5*, *CXCL6*, *CXCL7*, and *CXCL8*, the primary immune function of which is the regulation of neutrophil migration, as it controls the egress of these cells from the bone marrow, and their recruitment to sites of inflammation.[27] Collectively, our results revealed the immunomodulatory characteristics of neutrophils, as well as their crosstalk with MCs.

Monocytes/macrophages interact with MCs and neutrophils

The inflammatory response induced by PD within the peritoneal cavity contributes to the progressive damage of the peritoneum.[28] In response to injury, macrophages are stimulated to generate reactive oxygen species and recruit and activate additional MCs and fibroblasts to repair the peritoneum.[29] To ask whether macrophages affect the UF process, we next annotate monocytes/macrophages to investigate their differences between different PD statuses. The monocytes/macrophages were clustered into three subtypes, termed MRC1-macrophages, patrolling monocytes, and inflammatory monocytes (Figure 8A). Although the abundance of MRC1-macrophages and inflammatory monocytes were mainly accumulated in SV and gradually reduced from SV to LV_NOT_UF to LV_UF, notable change was observed only in MRC1-macrophages in the LV_UF group compared to the SV group (Figure 8B). Then, we performed a DEG analysis between LV_NOT_UF and LV_UF. The upregulated DEGs of monocytes/macrophages in the LV_UF group compared with the LV_NOT_UF group not only involved in pro-inflammatory response including neutrophil degranulation, inflammatory response, leukocyte migration, and cytokine-mediated signaling pathway but also associated with EMT progress, including positive regulation of cell migration, positive regulation of angiogenesis, and positive regulation of vascular endothelial growth factor (*VEGF*) production, as indicated by GO analysis based on DEGs (Figures 8C–8E). Considering the relationship between macrophages and fibrosis, we constructed a cellular interaction network map. The bubble plot showed the interrelationship among monocytes/macrophages and other cells in PDE (Figure S5), which demonstrated that MRC1-macrophages (Figure S5A) and inflammatory monocytes (Figure S5B) were positively correlated with fibroblasts and MCs. Meanwhile, we observed a strong interaction between monocytes/macrophages and neutrophils (Figure S5). In summary, these results revealed that monocytes/macrophages were involved in EMT and interacted with MCs and neutrophils.

DISCUSSION

We conducted a comprehensive analysis of PDE-derived cells based on scRNA-seq data. First, the cell populations in PDE were recognized as 8 main cell types based on the representative marker genes, including E-MCs, M-MCs, fibroblast, plasma B cells, cDC, pDC, T_NK cells, and myeloid. E-MCs from PDE were significantly increased in the LV_UF group compared with the SV and the LV_NOT_UF groups, possessed epithelial-like features, and displayed activated autophagy, pro-inflammation, and anti-inflammation. In contrast, the M-MCs and the *AQP1* expression in the peritoneal mesenchyme were reduced in the LV_UF group. The neutrophils and monocytes/macrophages responded to inflammation, connected with MC, and participated in EMT and fibrosis. Our study revealed PDE-derived cell compositions and transcription features in patients undergoing long-term PD with UF, demonstrating the dynamic changes of peritoneal cells and molecular mechanisms. This study provides scientific evidence for understanding UF and improving peritoneal membrane dysfunction at the cellular level, which may pave the way for the development of interventions aimed at mitigating peritoneal membrane dysfunction, thus improving the long-term viability and efficacy of PD as a renal replacement therapy.

The mesothelium surface layer formed by MCs is associated with preventing the formation of fibrous adhesions in the peritoneum. In 2003, Yáñez-Mó et al. demonstrated for the first time

Figure 5. M-MCs respond to UF through participating in EMT and fibrosis

(A) Proportion of cell number of M-MCs in the SV, LV_NOT_UF, and LV_UF groups. M-MCs are decreased in the LV_UF group compared with the SV group. The Wilcoxon Rank-Sum test was used to calculate the statistical difference. Data are represented as mean ± SD.

(B) The distribution of nine M-MC subclusters is displayed by the tSNE plot.

(C) Distribution of nine M-MC subclusters in cell pseudotime trajectory. Left: nine M-MC subclusters divided into five states; Middle: Distribution of nine M-MC subclusters in five developmental states; Right: Distribution of M-MCs in developmental trajectories in 16 samples.

(D) The expression distribution of cell markers (*COL1A1*, *COL3A1*, and *VIM*) of EMT in M-MCs, E-MCs, and fibroblast are represented in the UMAP plot.

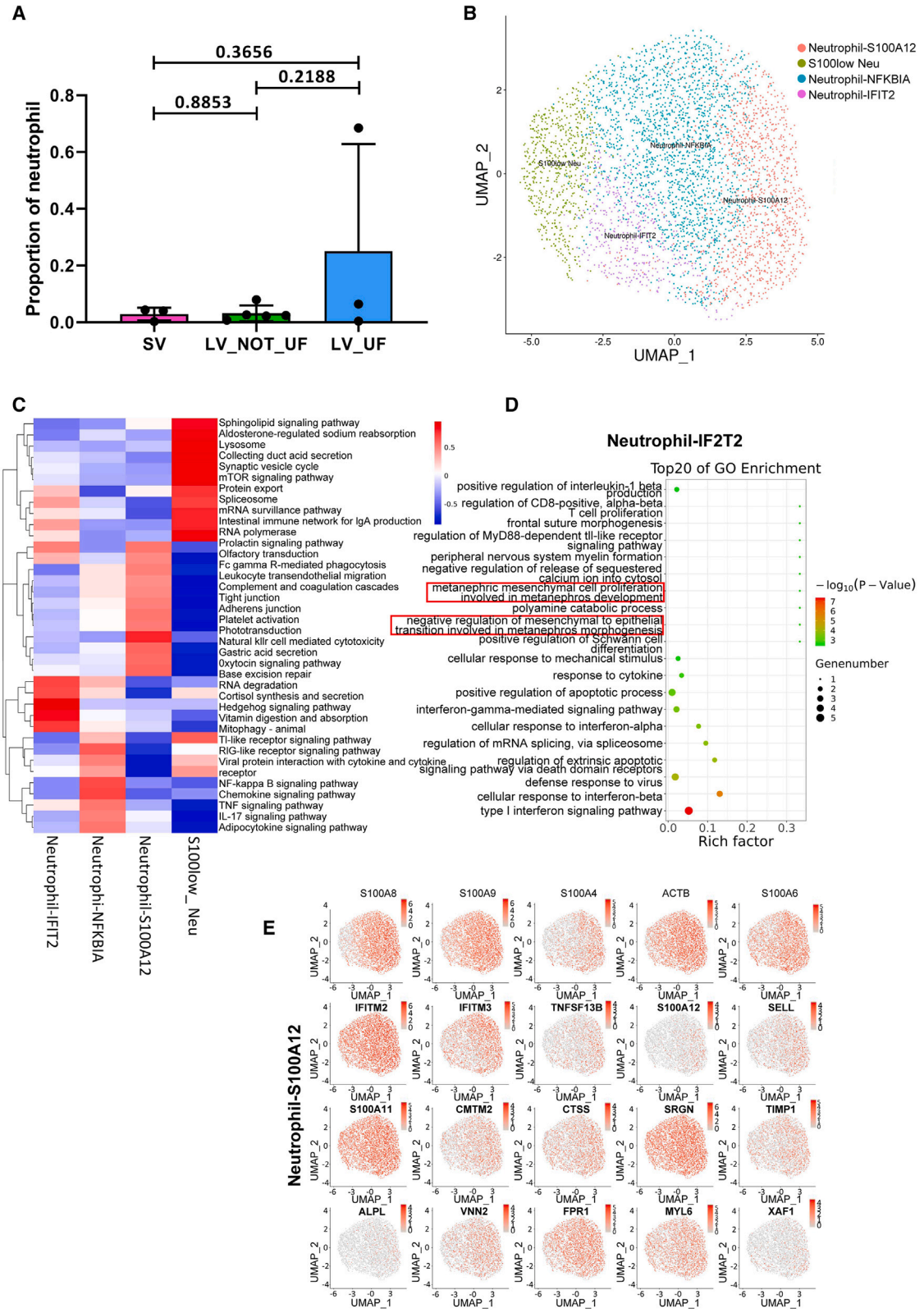

(legend on next page)

the presence of MCs undergoing mesenchymal transformation in effluent and peritoneal tissues of PD patients.[30] Subsequently, the researchers proposed to rename the mesenchymal transformation that occurs in different organs (e.g., lung, liver, or peritoneum) to a more appropriate term: mesothelial-to-mesenchymal transition (MMT).[31–33] During MMT, E-MCs gradually lose their epithelial-like features and apical-basolateral polarity and are transformed into M-MCs with a mesenchymal phenotype.[34] Peritonitis can exacerbate peritoneal injury, and in parallel with these peritoneal changes, mesothelial cells undergo MMT, which is associated with peritoneal deterioration in response to PD. Interestingly, MMT is a reversible process, meaning M-MCs can be converted to E-MCs. For example, Vargha et al. demonstrated that EMT conversion during PD can be reversed into the opposite direction by exogenously administered BMP-7.[35] Therefore, strategies targeting the MMT process may help to halt the progression of peritoneal fibrosis.

We found that E-MCs in PDE significantly increased in the LV_UF group, consistent with the reported studies that long-term PD and peritonitis induced the denudation of the mesothelium with features of epithelial cells.[36–38] After peritoneal injury, the mesothelial regeneration mechanism is initiated so that the MCs occur apoptosis and autophagy, and inflammatory cells release the cytokine to stimulate cells at the edge of the lesion to proliferate and accumulate on the wound surface within 48 h.[39–41] Inflammatory cells, particularly macrophages, could induce DNA synthesis and replication of mesothelial cells, while serosal healing is delayed after depletion of circulating monocytes.[40] Conversely, the mesenchymal-to-epithelial transition (MET) considers that the MCs gradually regained their simple squamous epithelial morphology and cellular organization.[42] The inflammation-stimulated MCs lost their contact with the basal lamina and each other and were first transformed into spindle-shaped cells in the EMT process.[43] Then, M-MCs gradually recovered the epithelial phenotypes after the peak inflammation time, accompanied by decreased organelles and increased autophagic structures in the cytoplasm.[44]

Moreover, we found that E-MCs exhibit pro-inflammatory and anti-inflammatory characteristics in the LV_UF group, which may imply that MC is undergoing the MMT transformation process. E-MCs are on a thin basement membrane covering the entire abdominal cavity, known as the "mesothelium". They are considered the first-line barrier to the abdominal cavity, providing a protective and non-adherent surface over the abdominal cavity and organs with anti-inflammatory properties to control peritoneal homeostasis.[45] However, during MMT, the loosening of tight adhesion between E-MCs creates conditions for invading reactive oxygen species and inflammatory factors, generating a pro-inflammatory and pro-fibrotic microenvironment in the peritoneal cavity.[46] MCs and surrounding macrophages can also produce large amounts of inflammatory factors (*IL-1β*, *TNF-α*, and *IL-6*) and pro-inflammatory mediators (chemokines, endogenous TLR ligands) in response to neutrophil stimulation.[47] Therefore, E-MCs are also considered to have pro-inflammatory properties. These suggest that intervention in the inflammatory phenotypic transformation in E-MCs could be a target for early intervention to maintain peritoneal integrity.

AQP1 is the only identified protein so far that is directly involved in PD fluid transport.[25] *AQP1* is constitutively expressed on the endothelial cells lining peritoneal capillaries and venules and has been confirmed to be the corresponding molecule for the ultra-small pore in the TPM model. In 2021, Morelle et al. found that *AQP1* promoter variant rs2075574 was associated with aquaporin-1 expression, ultrafiltration, and the prognosis of PD patients.[48] Zhang et al. confirmed the crucial role of endothelial *Aqp1* in ultrafiltration during PD using a *Aqp1*$^{-/-}$ mice.[49] However, few studies have focused on the expression of *AQP1* outside peritoneal vascular endothelial cells. In our study, vascular endothelial cells were not detected, but *AQP1* expression was detected in other non-immune cells, such as fibroblasts and mesothelial cells. Interestingly, further comparison of *AQP1* expression in non-immune cells among the three groups showed that the LV_UF group had the lowest *AQP1* expression and the LV_NOT_UF group had the highest *AQP1* expression. We speculate that, like the role of *AQP1* in vascular endothelial cells, *AQP1* expressed in peritoneal interstitial cells also mediates water filtration. High expression of *AQP1* in peritoneal interstitial cells may facilitate the passage of water through the interstitium to the peritoneal cavity.

Progressive membrane fibrosis can lead to UF. MMT is one of the essential mechanisms of peritoneal membrane fibrosis and can appear early after the initiation of PD.[33] Studies have shown that the degree of interstitial fibrosis increases with the prolongation of PD.[50] We found that the proportion of M-MCs in the LV_UF group decreased compared with the SV group, but it did not mean that the degree of interstitial fibrosis in the LV_UF group was lower than that in the SV group. Possible reasons for this finding are that the PD duration of our SV group (median: 5 months, range: 1 to 6 months) was much longer than the corresponding group of the previous studies, which enrolled patients who started PD within 1 week.[10,12] Long-time PD may allow more MMT to happen. In addition, as mentioned above, long-term inflammatory stimulation can cause M-MCs to undergo MMT,[44] leading to a decrease in M-MCs and an increase in E-MCs.

Peritoneal fibrosis has 2 cooperative parts: the fibrosis process and the inflammation. So, UF was accompanied by changes in the abundance of MCs and connected with inflammatory cells. We detected neutrophils in the effluent of patients accepting PD, which were associated with MCs and were elevated in the LV_UF group compared with the other groups.

Figure 6. Functional characteristics of neutrophil subclusters

(A) Proportion of neutrophils in the SV, LV_NOT_UF, and LV_UF groups. Neutrophils are elevated in the LV_UF group compared with the other groups, but the statistical difference was not significant. The *t*-test was used to calculate the statistical difference. Data are represented as mean ± SD.

(B) UMAP visualizes the distribution of four neutrophil subclusters.

(C) QuSAGE analysis of enrichment pathways of four neutrophil subclusters is shown by heatmap.

(D) The bubble map shows the top 20 GO enrichment terms of neutrophil-IFIT2 cell type based on marker genes.

(E) Expression of marker genes of neutrophil-S100A12 is represented by the UMAP plot.

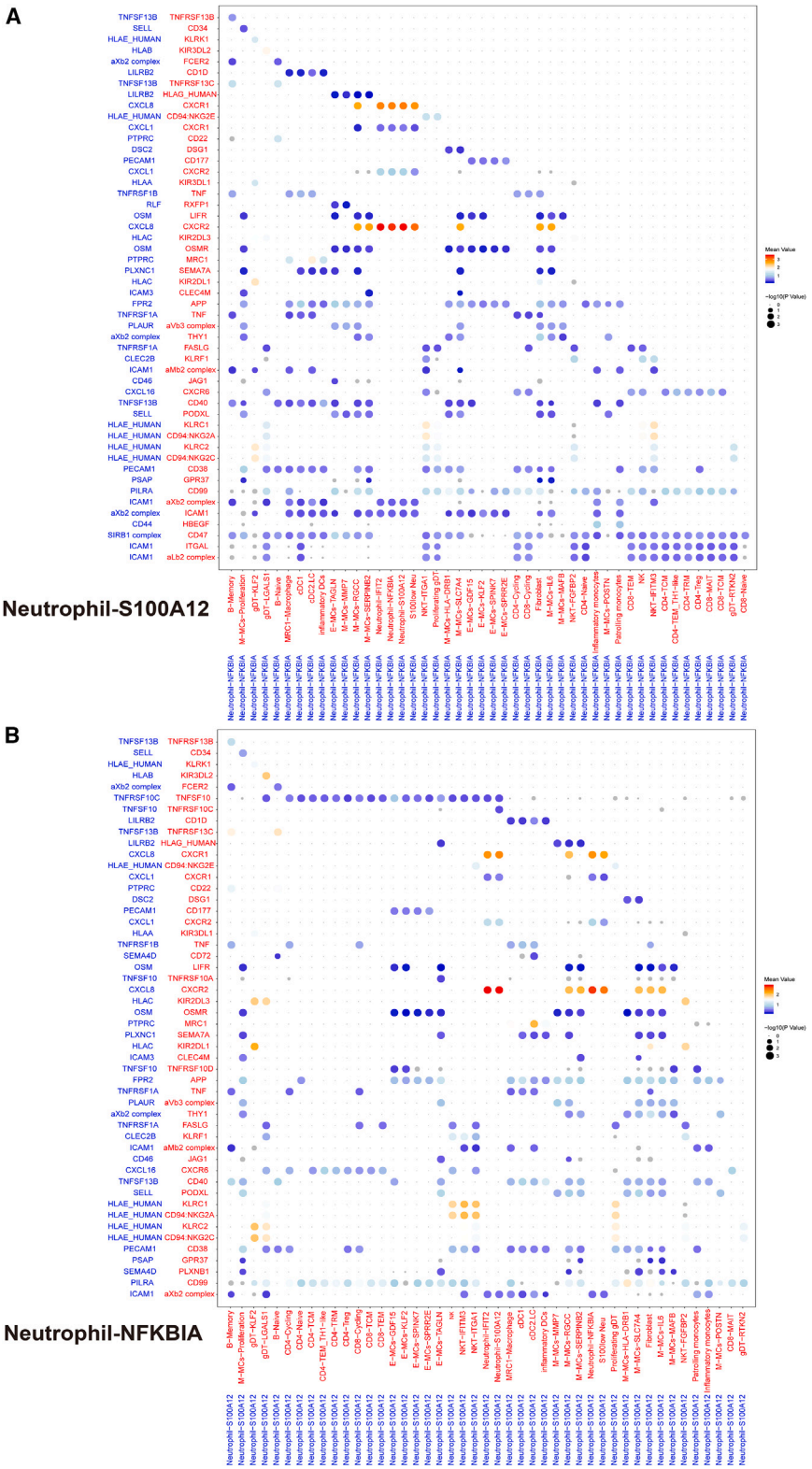

Figure 7. The crosstalk between neutrophil subclusters and other PDE-derived cells

(A and B) The bubble plot depicts ligand-receptor connections of neutrophil-S100A12 (A) and neutrophil-NFKBIA (B) with other PDE-derived cells. Bubble size indicates the statistical significance, and bubble color indicates the interaction level.

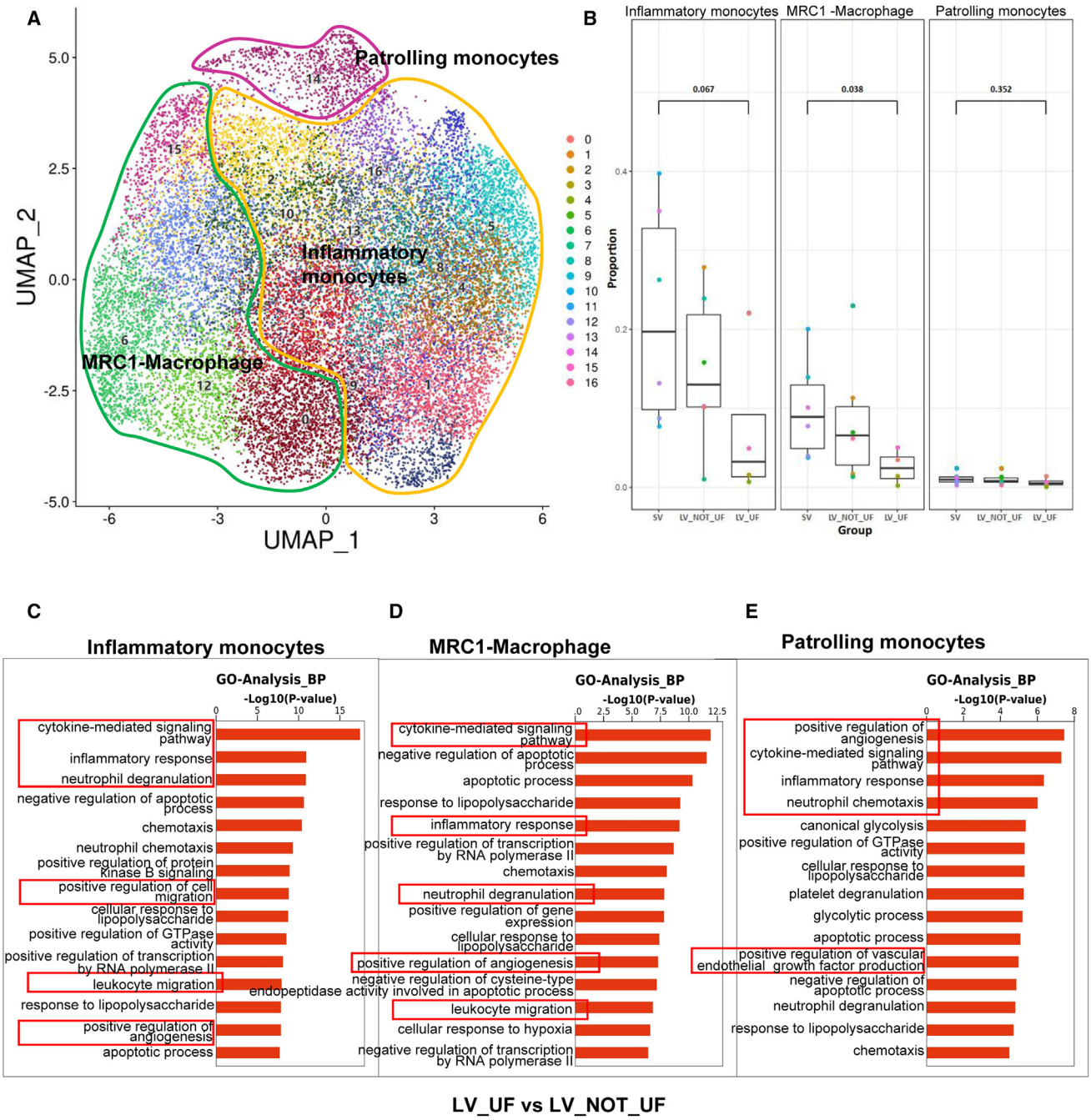

Figure 8. Monocytes/macrophages contribute to UF

(A) Monocytes/macrophages were re-clustered into three sub-cell types and displayed by a UMAP plot.

(B) Proportion of three monocyte/macrophage subclusters in the SV, LV_NOT_UF, and LV_UF groups. The Wilcoxon Rank-Sum test was used to calculate the statistical difference. Data are represented as mean ± SD.

(C–E) GO enrichment analysis shows function enrichment of DEGs between the LV_UF and the LV_NOT_UF groups of the inflammatory monocytes (C), MRC1-macrophages (D), and patrolling monocytes (E).

Inflammatory changes of early fibrotic events include the proliferation of ECM-secreting cells and the influx of mononuclear inflammatory infiltrates in the wound.[51] Neutrophils also release the toxic content of their granules, such as reactive oxygen and elastase, that injures the peritoneal membrane.[52] Studies on peritonitis have proven that once neutrophils enter the peritoneum, they undergo NETosis, which consists of releasing necrotic cell DNA, forming a net of aggregated neutrophils able

to trap and sequester microorganisms.[53] The influx and clearance of neutrophil is regulated by various cytokines produced by the peritoneum, such as *IL-6*, *IL-17*, and *IFN-γ*.[54] *IL-17* promotes the production of *CXCL1* by MCs by activating the expression of the transcription factor *SP1*, while *IFN-γ* inhibits *SP1* activation, and disruption of this balanced cross-regulation may lead to excessive or ineffective recruitment of neutrophils, subsequently leading to damage to the peritoneal membrane.[54]

Peritonitis remains a significant obstacle to the maintenance of long-term PD, and an unbalanced host peritoneal immune response may impair local anti-infective defenses, leading to treatment failure. We found that with the progression of SV to LV_NOT_UF to LV_UF, the proportion of three macrophage cell types (anti-inflammatory M2-like macrophages) gradually decreased, suggesting that as peritoneal dialysis progresses, the status and function of the local macrophage system in the peritoneum undergo dynamic changes. Numerous studies support our conclusions. For example, M2 macrophage reperfusion reduces histological damage, ECM deposition, and peritoneal ultrafiltration functional decline in mice compared to the M1 macrophage.[55] Liao et al. found that the distribution of macrophage subsets in different patients with peritonitis was significantly different, and heterogeneous macrophage subsets were associated with different PD outcomes.[56] In addition, the crosstalk between macrophage-mediated inflammation and fibroblasts leading to peritoneal fibrosis may be another significant factor of macrophage dynamic changes. *CCL17* is considered an essential mediator for switching inflammatory macrophages into pro-fibrotic phenotype macrophages and activating peritoneal fibroblasts, and supplementing with *CCL17* antibody can reduce macrophages, myofibroblasts, and fibrosis and improve peritoneal function.[57] Collectively, the heterogeneity of macrophage subpopulations revealed by our study may provide insights into the mechanism of UF in PD patients.

In conclusion, our analysis based on scRNA-seq data revealed dynamic changes in the cellular composition and function of individual peritoneal cell populations during PD. We demonstrated that most PDE-derived E-MCs were present in patients undergoing long-term PD with UF, and these E-MCs displayed enrichment in pathways of autophagy and inflammation. By contrast, the M-MC abundance and *AQP1* expression in PDE were reduced in the LV_UF group. Neutrophils and monocytes/macrophages were involved in inflammation response and interacted with MCs. These results highlight the potential value of identifying and developing therapeutic strategies for targeting MCs and inflammatory cells to prevent UF.

Limitations of the study

There are limitations in this study. First, the number of patients enrolled in each group was relatively small. This study recruited 16 patients, including 6 in the SV group, 6 in the LV_NOT_UF group, and 4 in the LV_UF group. It is known that sample sizes determine the number of cell populations. Larger cell numbers are preferred to enhance the reliability and validity of the findings. Despite the number of cells of each type being in hundreds or thousands, the sub-clustering of these cells results in a very small number of several cell subtypes. In addition, not every sample can identify all cell subtypes. Small cell numbers limit statistical power and reproducibility, increase variability, and cause sampling bias. Second, we collected PDE from PD patients, and the cells analyzed were the main cells shed from the peritoneum into the abdominal cavity, which may not accurately reflect the proportion of cells in the membrane. Third, sex, gender, or both may impact the results of the study, but we did not include these factors during the data processing. Finally, our findings need to be validated in larger cohorts and experiments. This can potentially further confirm our findings.

RESOURCE AVAILABILITY

Lead contact

Further information and any requests should be directed to and will be fulfilled by the lead contact,X.Y. (yxiao@mail.sysu.edu.cn).

Materials availability

The materials generated in this study are stored in our laboratory.

Data and code availability

- scRNA-seq data have been deposited at GEO and are publicly available as of the date of publication. Accession numbers are listed in the key resources table.
- This paper does not report the original code.
- All other data reported in this paper will be shared by the lead contact upon request.

ACKNOWLEDGMENTS

This study was supported by Guangdong Provincial Key Laboratory of Nephrology [2020B1212060028] and NHC Key Laboratory of Clinical Nephrology (Sun Yat-Sen University).

We are grateful for the service and technical support provided by NovelBio Co. Ltd. during the scRNA-seq process.

AUTHOR CONTRIBUTIONS

Y.X. and D.X.W. designed the research; Z.C.X., Y.H.J., and C.W. collected the data; W.H.S. and Y.C.Y. provided new reagents/analytic tools; D.X.W., L.J.X., and M.H.P. analyzed the data; D.X.W., Z.C.X., and Y.H.J. drafted the article. Y.X. and D.X.W. contributed significantly to editing the article. Y.X. was the supervision.

DECLARATION OF INTERESTS

The authors declare no competing interests.

STAR★METHODS

Detailed methods are provided in the online version of this paper and include the following:

- KEY RESOURCES TABLE
- EXPERIMENTAL MODEL AND SUBJECT DETAILS
- METHOD DETAILS
- QUANTIFICATION AND STATISTICAL ANALYSIS
  - Single-cell RNA-seq data processing
  - The cell types were clustered and visualized
  - Pseudotime analysis
  - Cell communication analysis
  - SCENIC analysis
  - QuSAGE analysis
  - Differential gene expression analysis
  - Gene enrichment analysis
- STATISTICAL ANALYSIS

SUPPLEMENTAL INFORMATION

Supplemental information can be found online at https://doi.org/10.1016/j.isci.2024.111383.

Received: November 6, 2023
Revised: July 2, 2024
Accepted: November 11, 2024
Published: November 13, 2024

REFERENCES

1. Aroeira, L.S., Aguilera, A., Sánchez-Tomero, J.A., Bajo, M.A., del Peso, G., Jiménez-Heffernan, J.A., Selgas, R., and López-Cabrera, M. (2007). Epithelial to mesenchymal transition and peritoneal membrane failure in peritoneal dialysis patients: pathologic significance and potential therapeutic interventions. J. Am. Soc. Nephrol. *18*, 2004–2013. https://doi.org/10.1681/ASN.2006111292.
2. Rippe, B., Stelin, G., and Haraldsson, B. (1991). Computer simulations of peritoneal fluid transport in CAPD. Kidney Int. *40*, 315–325. https://doi.org/10.1038/ki.1991.216.
3. Rippe, B. (2008). Free water transport, small pore transport and the osmotic pressure gradient three-pore model of peritoneal transport. Nephrol. Dial. Transplant. *23*, 2147–2153. https://doi.org/10.1093/ndt/gfn049.
4. Lee, K.J., Shin, D.A., Lee, H.S., and Lee, J.C. (2020). Computer simulations of steady concentration peritoneal dialysis. Perit. Dial. Int. *40*, 76–83. https://doi.org/10.1177/0896860819878635.
5. Flessner, M.F. (2008). Distributed model of peritoneal transport: implications of the endothelial glycocalyx. Nephrol. Dial. Transplant. *23*, 2142–2146. https://doi.org/10.1093/ndt/gfn055.
6. Flessner, M.F., Dedrick, R.L., and Schultz, J.S. (1984). A distributed model of peritoneal-plasma transport: theoretical considerations. Am. J. Physiol. *246*, R597–R607. https://doi.org/10.1152/ajpregu.1984.246.4.R597.
7. Lin, X., Lin, A., Ni, Z., Yao, Q., Zhang, W., Yan, Y., Fang, W., Gu, A., Axelsson, J., and Qian, J. (2010). Daily peritoneal ultrafiltration predicts patient and technique survival in anuric peritoneal dialysis patients. Nephrol. Dial. Transplant. *25*, 2322–2327. https://doi.org/10.1093/ndt/gfq001.
8. Stark, R., Grzelak, M., and Hadfield, J. (2019). RNA sequencing: the teenage years. Nat. Rev. Genet. *20*, 631–656. https://doi.org/10.1038/s41576-019-0150-2.
9. Hughes, T.K., Wadsworth, M.H., 2nd, Gierahn, T.M., Do, T., Weiss, D., Andrade, P.R., Ma, F., de Andrade Silva, B.J., Shao, S., Tsoi, L.C., et al. (2020). Second-Strand Synthesis-Based Massively Parallel scRNA-Seq Reveals Cellular States and Molecular Features of Human Inflammatory Skin Pathologies. Immunity *53*, 878–894.e7. https://doi.org/10.1016/j.immuni.2020.09.015.
10. Si, M., Wang, Q., Li, Y., Lin, H., Luo, D., Zhao, W., Dou, X., Liu, J., Zhang, H., Huang, Y., et al. (2019). Inhibition of hyperglycolysis in mesothelial cells prevents peritoneal fibrosis. Sci. Transl. Med. *11*, eaav5341. https://doi.org/10.1126/scitranslmed.aav5341.
11. Hu, W., Li, G., Dong, W., He, P., Liu, W., Wu, Y., Liang, H., Wen, F., Yu, F., Yin, Y., et al. (2023). Single-cell sequencing reveals peritoneal environment and insights into fibrosis in CAPD patients. iScience *26*, 106336. https://doi.org/10.1016/j.isci.2023.106336.
12. Zhang, J., Chen, Y., Chen, T., Miao, B., Tang, Z., Hu, X., Luo, Y., Zheng, T., and Na, N. (2021). Single-cell transcriptomics provides new insights into the role of fibroblasts during peritoneal fibrosis. Clin. Transl. Med. *11*, e321. https://doi.org/10.1002/ctm2.321.
13. Mutsaers, S.E. (2002). Mesothelial cells: their structure, function and role in serosal repair. Respirology *7*, 171–191. https://doi.org/10.1046/j.1440-1843.2002.00404.x.
14. Bragulla, H.H., and Homberger, D.G. (2009). Structure and functions of keratin proteins in simple, stratified, keratinized and cornified epithelia. J. Anat. *214*, 516–559. https://doi.org/10.1111/j.1469-7580.2009.01066.x.
15. Li, X., Yang, K.B., Chen, W., Mai, J., Wu, X.Q., Sun, T., Wu, R.Y., Jiao, L., Li, D.D., Ji, J., et al. (2021). CUL3 (cullin 3)-mediated ubiquitination and degradation of BECN1 (beclin 1) inhibit autophagy and promote tumor progression. Autophagy *17*, 4323–4340. https://doi.org/10.1080/15548627.2021.1912270.
16. Zhou, B., Liu, J., Kang, R., Klionsky, D.J., Kroemer, G., and Tang, D. (2020). Ferroptosis is a type of autophagy-dependent cell death. Semin. Cancer Biol. *66*, 89–100. https://doi.org/10.1016/j.semcancer.2019.03.002.
17. Xu, W.X., Zhang, J., Hua, Y.T., Yang, S.J., Wang, D.D., and Tang, J.H. (2020). An Integrative Pan-Cancer Analysis Revealing LCN2 as an Oncogenic Immune Protein in Tumor Microenvironment. Front. Oncol. *10*, 605097. https://doi.org/10.3389/fonc.2020.605097.
18. Leite Dantas, R., Bettenworth, D., Varga, G., Weinhage, T., Wami, H.T., Dobrindt, U., Roth, J., Vogl, T., Ludwig, S., and Wixler, V. (2020). Spontaneous onset of TNFalpha-triggered colonic inflammation depends on functional T lymphocytes, S100A8/A9 alarmins, and MHC H-2 haplotype. J. Pathol. *251*, 388–399. https://doi.org/10.1002/path.5473.
19. Zheng, J., Wang, J., Liu, H., Chen, F., Wang, H., Chen, S., Xie, J., Zheng, Z., and Li, Z. (2022). Alarmins S100A8/A9 promote intervertebral disc degeneration and inflammation-related pain in a rat model through toll-like receptor-4 and activation of the NF-kappaB signaling pathway. Osteoarthritis Cartilage *30*, 998–1011. https://doi.org/10.1016/j.joca.2022.03.011.
20. Lu, Z., and Sun, F. (2022). Downregulated TICAM1 is a prognostic biomarker and associated with immune tolerance of Wilms tumor patients. BMC Med. Genom. *15*, 174. https://doi.org/10.1186/s12920-022-01326-5.
21. Bao, N., Fu, B., Zhong, X., Jia, S., Ren, Z., Wang, H., Wang, W., Shi, H., Li, J., Ge, F., et al. (2023). Role of the CXCR6/CXCL16 axis in autoimmune diseases. Int. Immunopharm. *121*, 110530. https://doi.org/10.1016/j.intimp.2023.110530.
22. Mi, J., Liu, Z., Pei, S., Wu, X., Zhao, N., Jiang, L., Zhang, Z., and Bai, X. (2022). Mendelian randomization study for the roles of IL-18 and IL-1 receptor antagonist in the development of inflammatory bowel disease. Int. Immunopharm. *110*, 109020. https://doi.org/10.1016/j.intimp.2022.109020.
23. Vilar, K.d.M., Pereira, M.C., Tavares Dantas, A., de Melo Rêgo, M.J.B., Pitta, I.D.R., Pinto Duarte, Â.L.B., and da Rocha Pitta, M.G. (2019). Galectin-9 gene (LGALS9) polymorphisms are associated with rheumatoid arthritis in Brazilian patients. PLoS One *14*, e0223191. https://doi.org/10.1371/journal.pone.0223191.
24. Ni, J., Verbavatz, J.M., Rippe, A., Boisdé, I., Moulin, P., Rippe, B., Verkman, A.S., and Devuyst, O. (2006). Aquaporin-1 plays an essential role in water permeability and ultrafiltration during peritoneal dialysis. Kidney Int. *69*, 1518–1525. https://doi.org/10.1038/sj.ki.5000285.
25. Devuyst, O., and Rippe, B. (2014). Water transport across the peritoneal membrane. Kidney Int. *85*, 750–758. https://doi.org/10.1038/ki.2013.250.
26. Masola, V., Bonomini, M., Borrelli, S., Di Liberato, L., Vecchi, L., Onisto, M., Gambaro, G., Palumbo, R., and Arduini, A. (2022). Fibrosis of Peritoneal Membrane as Target of New Therapies in Peritoneal Dialysis. Int. J. Mol. Sci. *23*, 4831. https://doi.org/10.3390/ijms23094831.
27. Steele, C.W., Karim, S.A., Leach, J.D.G., Bailey, P., Upstill-Goddard, R., Rishi, L., Foth, M., Bryson, S., McDaid, K., Wilson, Z., et al. (2016). CXCR2 Inhibition Profoundly Suppresses Metastases and Augments Immunotherapy in Pancreatic Ductal Adenocarcinoma. Cancer Cell *29*, 832–845. https://doi.org/10.1016/j.ccell.2016.04.014.
28. Tomasz, J., and Andrzej, B. (2022). Hyaluronan reduces colitis-induced intraperitoneal inflammation during peritoneal dialysis. Perit. Dial. Int. *42*, 212–217. https://doi.org/10.1177/08968608211014568.

29. Capobianco, A., Cottone, L., Monno, A., Manfredi, A.A., and Rovere-Querini, P. (2017). The peritoneum: healing, immunity, and diseases. J. Pathol. *243*, 137–147. https://doi.org/10.1002/path.4942.

30. Yáñez-Mó, M., Lara-Pezzi, E., Selgas, R., Ramírez-Huesca, M., Domínguez-Jiménez, C., Jiménez-Heffernan, J.A., Aguilera, A., Sánchez-Tomero, J.A., Bajo, M.A., Alvarez, V., et al. (2003). Peritoneal dialysis and epithelial-to-mesenchymal transition of mesothelial cells. N. Engl. J. Med. *348*, 403–413. https://doi.org/10.1056/NEJMoa020809.

31. Mubarak, K.K., Montes-Worboys, A., Regev, D., Nasreen, N., Mohammed, K.A., Faruqi, I., Hensel, E., Baz, M.A., Akindipe, O.A., Fernandez-Bussy, S., et al. (2012). Parenchymal trafficking of pleural mesothelial cells in idiopathic pulmonary fibrosis. Eur. Respir. J. *39*, 133–140. https://doi.org/10.1183/09031936.00141010.

32. Li, Y., Wang, J., and Asahina, K. (2013). Mesothelial cells give rise to hepatic stellate cells and myofibroblasts via mesothelial-mesenchymal transition in liver injury. Proc. Natl. Acad. Sci. USA *110*, 2324–2329. https://doi.org/10.1073/pnas.1214136110.

33. Loureiro, J., Sandoval, P., del Peso, G., Gónzalez-Mateo, G., Fernández-Millara, V., Santamaria, B., Bajo, M.A., Sánchez-Tomero, J.A., Guerra-Azcona, G., Selgas, R., et al. (2013). Tamoxifen ameliorates peritoneal membrane damage by blocking mesothelial to mesenchymal transition in peritoneal dialysis. PLoS One *8*, e61165. https://doi.org/10.1371/journal.pone.0061165.

34. López-Cabrera, M. (2014). Mesenchymal Conversion of Mesothelial Cells Is a Key Event in the Pathophysiology of the Peritoneum during Peritoneal Dialysis. Adv Med. *2014*, 473134.

35. Vargha, R., Endemann, M., Kratochwill, K., Riesenhuber, A., Wick, N., Krachler, A.M., Malaga-Dieguez, L., and Aufricht, C. (2006). Ex vivo reversal of in vivo transdifferentiation in mesothelial cells grown from peritoneal dialysate effluents. Nephrol. Dial. Transplant. *21*, 2943–2947. https://doi.org/10.1093/ndt/gfl355.

36. Liu, Y., Li, J.F., Liu, H., Liu, F.Y., Peng, Y.M., Liu, Y.H., Cheng, M.C., Chen, G.C., and Zhou, X. (2014). Functional and structural alterations of peritoneum and secretion of fibrotic cytokines in rats caused by high glucose peritoneal dialysis solutions. Ren. Fail. *36*, 292–299. https://doi.org/10.3109/0886022X.2013.844645.

37. Yung, S., and Chan, T.M. (2012). Pathophysiological changes to the peritoneal membrane during PD-related peritonitis: the role of mesothelial cells. Mediat. Inflamm. *2012*, 484167. https://doi.org/10.1155/2012/484167.

38. Lee, E.A., Oh, J.H., Lee, H.A., Kim, S.I., Park, E.W., Park, K.B., and Park, M.S. (2001). Structural and functional alterations of the peritoneum after prolonged exposure to dialysis solutions: role of aminoguanidine. Perit. Dial. Int. *21*, 245–253.

39. Rodgers, K.E., and diZerega, G.S. (1992). Modulation of peritoneal reepithelialization by postsurgical macrophages. J. Surg. Res. *53*, 542–548. https://doi.org/10.1016/0022-4804(92)90104-8.

40. Mutsaers, S.E., Whitaker, D., and Papadimitriou, J.M. (2002). Stimulation of mesothelial cell proliferation by exudate macrophages enhances serosal wound healing in a murine model. Am. J. Pathol. *160*, 681–692. https://doi.org/10.1016/S0002-9440(10)64888-2.

41. Mutsaers, S.E., Whitaker, D., and Papadimitriou, J.M. (2000). Mesothelial regeneration is not dependent on subserosal cells. J. Pathol. *190*, 86–92. https://doi.org/10.1002/(SICI)1096-9896(200001)190:1<86::AID-PATH493>3.0.CO;2-G.

42. Zsiros, V., and Kiss, A.L. (2020). Cellular and molecular events of inflammation induced transdifferentiation (EMT) and regeneration (MET) in mesenteric mesothelial cells. Inflamm. Res. *69*, 1173–1179. https://doi.org/10.1007/s00011-020-01400-7.

43. Balogh, P., Szabó, A., Katz, S., Likó, I., Patócs, A., and Kiss, A.L. (2013). Estrogen receptor alpha is expressed in mesenteric mesothelial cells and is internalized in caveolae upon Freund's adjuvant treatment. PLoS One *8*, e79508. https://doi.org/10.1371/journal.pone.0079508.

44. Zsiros, V., Katz, S., Dóczi, N., and Kiss, A.L. (2017). Autophagy is the key process in the re-establishment of the epitheloid phenotype during mesenchymal-epithelial transition (MET). Exp. Cell Res. *352*, 382–392. https://doi.org/10.1016/j.yexcr.2017.02.031.

45. Yung, S., and Chan, T.M. (2007). Mesothelial cells. Perit. Dial. Int. *27*, S110–S115.

46. Kang, D.H. (2020). Loosening of the mesothelial barrier as an early therapeutic target to preserve peritoneal function in peritoneal dialysis. Kidney Res. Clin. Pract. *39*, 136–144. https://doi.org/10.23876/j.krcp.20.052.

47. Strippoli, R., Moreno-Vicente, R., Battistelli, C., Cicchini, C., Noce, V., Amicone, L., Marchetti, A., del Pozo, M.A., and Tripodi, M. (2016). Molecular Mechanisms Underlying Peritoneal EMT and Fibrosis. Stem Cell. Int. *2016*, 3543678. https://doi.org/10.1155/2016/3543678.

48. Morelle, J., Marechal, C., Yu, Z., Debaix, H., Corre, T., Lambie, M., Verduijn, M., Dekker, F., Bovy, P., Evenepoel, P., et al. (2021). AQP1 Promoter Variant, Water Transport, and Outcomes in Peritoneal Dialysis. N. Engl. J. Med. *385*, 1570–1580. https://doi.org/10.1056/NEJMoa2034279.

49. Zhang, W., Freichel, M., van der Hoeven, F., Nawroth, P.P., Katus, H., Kälble, F., Zitron, E., and Schwenger, V. (2016). Novel Endothelial Cell-Specific AQP1 Knockout Mice Confirm the Crucial Role of Endothelial AQP1 in Ultrafiltration during Peritoneal Dialysis. PLoS One *11*, e0145513. https://doi.org/10.1371/journal.pone.0145513.

50. Zhou, Q., Bajo, M.A., Del Peso, G., Yu, X., and Selgas, R. (2016). Preventing peritoneal membrane fibrosis in peritoneal dialysis patients. Kidney Int. *90*, 515–524. https://doi.org/10.1016/j.kint.2016.03.040.

51. Wick, G., Backovic, A., Rabensteiner, E., Plank, N., Schwentner, C., and Sgonc, R. (2010). The immunology of fibrosis: innate and adaptive responses. Trends Immunol. *31*, 110–119. https://doi.org/10.1016/j.it.2009.12.001.

52. Nathan, C. (2006). Neutrophils and immunity: challenges and opportunities. Nat. Rev. Immunol. *6*, 173–182. https://doi.org/10.1038/nri1785.

53. Korabecna, M., and Tesar, V. (2017). NETosis provides the link between activation of neutrophils on hemodialysis membrane and comorbidities in dialyzed patients. Inflamm. Res. *66*, 369–378. https://doi.org/10.1007/s00011-016-1010-6.

54. Catar, R.A., Chen, L., Cuff, S.M., Kift-Morgan, A., Eberl, M., Kettritz, R., Kamhieh-Milz, J., Moll, G., Li, Q., Zhao, H., et al. (2020). Control of neutrophil influx during peritonitis by transcriptional cross-regulation of chemokine CXCL1 by IL-17 and IFN-γ. J. Pathol. *251*, 175–186. https://doi.org/10.1002/path.5438.

55. Li, Q., Zheng, M., Liu, Y., Sun, W., Shi, J., Ni, J., and Wang, Q. (2018). A pathogenetic role for M1 macrophages in peritoneal dialysis-associated fibrosis. Mol. Immunol. *94*, 131–139. https://doi.org/10.1016/j.molimm.2017.12.023.

56. Liao, C.-T., Andrews, R., Wallace, L.E., Khan, M.W.A., Kift-Morgan, A., Topley, N., Fraser, D.J., and Taylor, P.R. (2017). Peritoneal macrophage heterogeneity is associated with different peritoneal dialysis outcomes. Kidney Int. *91*, 1088–1103. https://doi.org/10.1016/j.kint.2016.10.030.

57. Chen, Y.T., Hsu, H., Lin, C.C., Pan, S.Y., Liu, S.Y., Wu, C.F., Tsai, P.Z., Liao, C.T., Cheng, H.T., Chiang, W.C., et al. (2020). Inflammatory macrophages switch to CCL17-expressing phenotype and promote peritoneal fibrosis. J. Pathol. *250*, 55–66. https://doi.org/10.1002/path.5350.

STAR★METHODS

KEY RESOURCES TABLE

REAGENT or RESOURCE	SOURCE	IDENTIFIER
Biological samples		
Patients-derived peritoneal dialysis effluent	The First Affiliated Hospital of Sun Yat-sen University	https://www.fahsysu.org.cn/home
Critical commercial assays		
Chromium Single Cell 3′V3.1 kit	10× Genomics	PN-1000268
Qubit High Sensitivity DNA assay	Thermo Fisher Scientific	Q33231
Deposited data		
Raw and processed scRNA-seq data	GEO database (https://www.ncbi.nlm.nih.gov/geo/query/acc.cgi?acc=GSE248762)	GSE248762
Software and algorithms		
Ensemble	https://www.ensembl.org/index.html?redirect=no	version 9.1
Cell Ranger	10x Genomics	version 3.1.0
Seurat package	https://satijalab.org/seurat/	version 4.0.3
R software package Seurat	satijalab	version 3.1.1
Monocle2	http://cole-trapnell-lab.github.io/monocle-release	version 0.9.5
CellPhoneDB	https://www.cellphonedb.org/	version 4.1.0
pySCENIC	https://scenic.aertslab.org/	version 0.12.1
QuSAGE	Bioconductor	version 2.16.1
NCBI	http://www.ncbi.nlm.nih.gov/	N/A
UniProt	http://www.uniprot.org/	N/A
Gene Ontology	http://www.geneontology.org/	N/A
Other		
Illumina NovaSeq	Illumina	Illumina NovaSeq 6000
Bioanalyzer	Agilent	Bioanalyzer 2100

EXPERIMENTAL MODEL AND SUBJECT DETAILS

PD patients were screened regularly and followed up at The First Affiliated Hospital of Sun Yat-sen University from June 1, 2021, to June 1, 2022. Our study was supported by the Research Ethics Committee (IRB Number: IIT-2022-633) of The First Affiliated Hospital of Sun Yat-sen University. Inclusion criteria of patients: (1) Regular follow-up at the PD center in the hospital; (2) Age greater than 18 years old; (3) Be willing to participate in this study and sign an informed consent form. Exclusion criteria of patients: (1) Patients after kidney transplantation or long-term hemodialysis converts to PD; (2) History of peritonitis for 4 weeks before the collection of dialysate samples; (3) Patients with a history of malignant tumors; (4) Patients with catheter-related UF dysfunction or dialysate leakage occurred; (5) Patients with colitis ulcerosa or abdominal organ cancer.

Participants were categorized based on the timing of PD initiation and the volume of ultrafiltration associated with PD treatment. The allocation criteria for the subjects are as follows: 1) SV group: patients received PD for less than 6 months; 2) LV_NOT_UF group: patients received PD for more than 90 months, and the modified PET (Mod-PET) test showed that the ultrafiltration volume was greater than 400 mL; 3) LV_UF group: patients received PD for more than 90 months, Mod-PET test showed that the ultrafiltration volume was less than 400 mL.

For single-cell RNA-seq, we collected overnight effluent from 16 PD patients within 1 h of *ex vivo*, including 6 SV patients, 6 patients in the LV_NOT_UF group, and 4 patients in the LV_UF group. The age, sex, and PD terms of the patients were collected. The detailed basic clinical features and concentration of glucose dialysate of 16 PD patients are shown in Table S1.

A Mod-PET test was performed at the patient's follow-up visit to assess whether they had ultrafiltration failure using 4.25% glucose dialysate. Peritoneal dialysate (PD solution contains 2 L of 4.25% glucose) was used to stay in the abdomen for 4 h. Collecting dialysate at 0 h, 1 h, and 4 h, and blood samples at l h after abdominal dialysis, which was determined the concentration of creatinine, glucose, and sodium. Meanwhile, counting the ultrafiltration volume, 4h D/P Cr, sodium difference ($[Na^+]t = 0$ - $[Na^+]t = 60$ min), sodium sieving ratio (1 - $[Na^+]t = 60$ min/$[Na^+]t = 0$).

METHOD DETAILS

After centrifugation of PDE at 500g for 10 min, the cell pellet was incubated on ice with 2 mL of cell lysate for 8 min. Cells were washed with phosphate-buffered saline (PBS) containing 0.4% BSA and centrifuged at 400g for 5 min. Then, cells were resuspended in PBS containing 0.4% BSA, and the activity was measured. Countstar automated cell counter was used to calculate cell numbers, which required more than 50,000 cells. Moreover, the quality of cells demanded that the concentration of cell suspension was 700–1200 cells/μL and the cell activity >80%.

QUANTIFICATION AND STATISTICAL ANALYSIS

Single-cell RNA-seq data processing

scRNA-seq was conducted by Jiangxi NovelBio in China. The scRNA-seq library was generated by the Chromium Single Cell 3′V3.1 kit (10× Genomics, Pleasanton, California, USA) and the 10× Genomics Chromium Controller instrument. Briefly, cells were concentrated to approximately 1000 cells/uL and loaded into each channel to generate single-cell Gel Bead-In-Emulsions (GEMs). After the RT step, GEMs were broken, and barcoded cDNA was purified and amplified. The amplified barcoded cDNA was fragmented, A-tailed, and ligated with adaptors, and the index PCR was amplified. The final libraries were quantified using the Qubit High Sensitivity DNA assay (Thermo Fisher Scientific), and the size distribution of the libraries was determined using a High Sensitivity DNA chip on a Bioanalyzer 2200 (Agilent). All libraries were sequenced by Illumina sequencer (Illumina, San Diego, CA) on a 150 bp paired-end run.

The fastp with default parameter was applied to filter the adaptor sequence and remove the low-quality reads to achieve clean data. The clean data was matched with the Ensemble reference genome (GRCh38 Ensemble, v9.1) using Cell Ranger (v3.1.0) based on the STAR Methods, including exons, introns, intergenic regions, and full-length transcript regions. As a quality control, cells with expressed genes $\geq$200 and mitochondrial unique molecular identifier (UMI) rate $\leq$20% were selected. Seurat package (v4.0.3, https://satijalab.org/seurat/) was used for cell normalization and regression based on the expression table according to the UMI counts of each sample and percent of mitochondria rate to obtain the scaled data. Since samples were processed and sequenced in batches, we used mutual nearest-neighbour (MNN) to remove the potential batch effect. The raw data of scRNA-seq has been released to NCBI under the accession number GSE248762.

The cell types were clustered and visualized

Principal component analysis (PCA) was performed based on the top 2,000 genes with significant differences. Then, the top 10 principal components were visualized by dimensionality reduction using the unified manifold approximation and projection (UMAP). We used the R software package Seurat (v3.1.1) to analyze scRNA-seq data, and the marker gene was calculated using the FindAllMarkers function after Wilcoxon Rank-Sum tested the algorithm and default parameters. Re-tSNE analysis was performed to identify the cell type and select a cell population with the same cell type.

Pseudotime analysis

We applied the Single-Cell Trajectories analysis utilizing Monocle2 (http://cole-trapnell-lab.github.io/monocle-release) using DDR-Tree and default parameter (the cut-off q value was 0.0001, the top gene number was 1000). Before the Monocle analysis, we selected marker genes of the Seurat clustering result and raw expression counts of the cell passed filtering. Based on the pseudo-time analysis, branch expression analysis modeling (BEAM Analysis) was applied for branch fate-determined gene analysis.

Cell communication analysis

To enable a systematic analysis of cell-cell communication molecules, we applied cell communication analysis based on the CellPhoneDB, a public repository of ligands, receptors, and their interactions. Membrane, secreted, and peripheral proteins of the cluster of different time points were annotated. Significant mean and Cell Communication significance (p value <0.05) were calculated based on the interaction and the normalized cell matrix achieved by Seurat Normalization.

SCENIC analysis

To assess transcription factor regulation strength, we applied the Single-cell regulatory network inference and clustering (pySCENIC, v0.9.5) workflow, using the 20-thousand motifs database for RcisTarget and GRNboost., RANK_THRESHOLD:5000, NES_THRESHOLD:3, AUC_THRESHOLD:0.05.

QuSAGE analysis

To characterize the relative activation of a given gene set, such as pathway activation, we performed QuSAGE (v2.16.1) analysis under the following criteria: FDR <0.05.

Differential gene expression analysis

To identify differentially expressed genes among samples, the function FindMarkers with Wilcoxon Rank-Sum test algorithm was used under the following criteria: 1. lnFC >0.25; 2. p value <0.05; 3. min.pct >0.1.

Gene enrichment analysis

We downloaded Gene ontology (GO) annotations from NCBI (http://www.ncbi.nlm.nih.gov/), UniProt (http://www.uniprot.org/), and the Gene Ontology (http://www.geneontology.org/) to elucidate the gene function of marker genes and differentially expressed genes (DEGs). Pathway analysis was performed to identify enriched pathways of marker genes and DEGs according to the Kyoto Encyclopedia of Genes and Genomes (KEGG) database. Fisher's exact test recognized the significant GO terms and pathways, and the false discovery rate (FDR) was used to correct the p value.

STATISTICAL ANALYSIS

The Wilcoxon Rank-Sum test and unpaired t-test were used to calculate statistical differences between the two groups. A p value <0.05 is considered as a statistical difference. $^{***}p < 0.001$.